



Research Article

CHEMISTRY

In₂O₃/Polyaniline nanocomposite as an innovative and effective adsorbent for removing Acid blue 25 from wastewater

Mohamed A. Salem^{1*}, Mohamed A. El-Damanhoury¹, Ahmed M. Omer², Marwa A. El-Ghobashy^{1*}

¹ Chemistry Department, Faculty of Science, Tanta University, Tanta 31527, Egypt

² Polymer Materials Research Department, Advanced Technology and New Materials Research Institute (ATNMRI), the City of Scientific Research and Technological Applications (SRTA-City), New Borg El-Arab City, P.O. Box: 21934, Alexandria, Egypt

Corresponding Author: Mohamed A. Salem
Marwa A. El-Ghobashy

e-mail: masalem@science.tanta.edu.eg

e-mail: marwa_elghobashy@science.tanta.edu.eg

Received: 24/ 5/2023

Accepted: 8/ 6/2023

KEY WORDS

Adsorption,
Polyaniline,
Nanocomposites,
Acid blue 25,
In₂O₃

ABSTRACT

The jeopardy of hazardous synthetic dye wastes to the environment and human health has rapidly increased. In this investigation, a nanocomposite of In₂O₃/Polyaniline (In₂O₃/PANI) has been fabricated to remove the noxious anionic acid blue 25 (AB25) dye by adsorption. Various characterization techniques including FT-IR, XRD, SEM, EDX, TEM, BET, and Zeta potential analysis were carefully used to verify that the nanocomposite was successfully synthesized. The developed adsorbent features a porous structure with an average particle size of 58.43 nm. The results revealed that only 0.007 g of the nanocomposite can efficiently remove 95.5% of AB25 within 90 min. Kinetically, the adsorption results followed the pseudo-second-order model. In addition, the adsorption data matched well with the Langmuir and Toth isotherm models giving a maximum adsorption capacity of 253.36 mg/g. Thermodynamically, the adsorption process was spontaneous and endothermic. Notably, the nanocomposite displayed auspicious adsorption selectivity towards the anionic AB25 compared to the cationic methylene blue dye (MB). Interestingly, the as-fabricated In₂O₃/PANI nanocomposite retained satisfactory adsorption characteristics after five consecutive cycles with removal percentage exceeding 83%, suggesting that this method is a viable and effective option for eliminating harmful anionic dyes from aquatic environments.

Introduction

The pollution of water has turned into a significant issue in the environment. The pollutant removal from water is necessary to produce fresh water (Kumar, Muralidhara et al., 2013). Among the numerous pollutants are dyes which are present in the wastewater (Al-Musawi, Rajiv et al., 2021). Due to the toxicity and carcinogenic effect of dyes, their existence is hurtful to the environment (Ayad, El-Nasr et al., 2012). Dyes are broadly utilized in plastics, paints, photographs, food, papers, textile, cosmetics, and pharmaceutical products (Zhao, Chen et al., 2017). The anionic dye Acid blue 25 is widely used for dyeing silk, nylon, and wool fibers (Daneshvar, Sohrabi et al., 2014). Several treatment methods are potentially used for wastewater purification from dyes. These methods are chemical, physical, and biological (Kareem, Abd Alrazak et al., 2016). Due to the stability of dyes against light, the physical methods have been recognized as the most efficient in achieving the desired water quality. Adsorption as a physical technique has been widely applied to remove dyes from wastewater due to its high efficiency, cost-effectiveness, and simplicity (Ali, Kon'kova et al., 2022). Polymers are used to adsorb various pollutants from aqueous solutions

because of their high performance, excellent mechanical rigidity, economic regeneration and high environmental stability (Samadi, Xie et al., 2021). Polyaniline has been extensively studied as an adsorbent for the removal of aqueous pollutants (Benykhlef, Bekhoukh et al., 2016). Polyaniline/metal oxides (TiO₂, ZnO, Fe₂O₃, and SiO₂) composites have been utilized in sensors (Song, Wei et al., 2022), biosensors (Sharma, Dutta et al., 2022), rechargeable batteries (Yang, Lao et al., 2022), fuel cells (Dessie, Tadesse et al., 2022), and solar cells (Ferrag, Noroozifar et al., 2022). Some of these composites as adsorbents have been applied in removing heavy metals and dyes and from aqueous media (Mohanty and Biswal, 2022). Among these composites are the PANI/ZnO, PANI/clay, and PANI/Fe₃O₄ which were used respectively for the removal of Acid Blue 25, Acid green 25, and Congo red (Gilja, Vrban et al., 2018, Kalotra and Mehta 2021, Teng, Bryan et al. 2021).

Because of the high, fast response, and recovery time of the metal oxide semiconductors, they are greatly applied in pollutant degradation, CO₂ reduction, photocatalytic degradation, electrode materials, and gas sensors (Lin, Wang et al., 2018). The direct and indirect band gaps of the semiconductor indium

oxide (In₂O₃) are 3.75 and 2.6 eV, respectively (Yang, Hong et al., 2021). The locations of the valence and conduction bands of In₂O₃ match well with the redox potentials of the water. Recent research on doped and non-doped In₂O₃ has dealt with the synthesis of In₂O₃ in various nano-structural shapes (Bagheri-Mohagheghi, Shahtahmasebi et al., 2009). A variety of synthesis routes, namely sol-gel (Sridhar B, Husain et al., 2016), hydrothermal (Zhao, Zheng et al., 2012), co-precipitation (Senthilkumar, Senthil et al., 2012), and emulsion (Jiang, Liu et al., 2021) have been used to synthesize In₂O₃ nanoparticles. The sol-gel and hydrothermal routes are simple, low-cost, and useful to control the size and shape of the particle (Pantilimon, Kang et al. 2016). The In₂O₃/Halloysite as an adsorbent was utilized to remove tetracycline (Zhang, Wang et al., 2021). The modified forms of In₂O₃ such as platinum/In₂O₃, Ni₂P/In₂O₃, TiO₂/In₂O₃, and In₂O₃/Bi₄O₇ nanocomposites were used as photocatalysts for the degradation of perfluorooctanoic acid, Rhodamine B, Sudan I and doxycycline hydrochloride, respectively (Skorb, Ustinovich et al., 2008, Xu, Qiu et al., 2017, Pan, Qian et al., 2021, Yang, Hong et al., 2021). Herein, the In₂O₃/polyaniline nanocomposite was fabricated for the first time via the

polymerization of aniline in the existence of In₂O₃ nanoparticles. The developed adsorbent aptitude has been examined for the adsorptive elimination of anionic AB25 dye using batch adsorption technique under the effect of several parameters. Additionally, the adsorption kinetics, adsorption isotherms, and thermodynamic determination were executed to investigate the adsorption process. Moreover, both anionic AB25 and cationic MB dyes have been used to evaluate the adsorbent selectivity. Further, the ability of the nanocomposite to be recycled for multiple cycles was also evaluated.

Experimental

Materials

Indium (III) nitrate hydrate (In(NO₃)₃.xH₂O, 99.9 %) was supplied from Fluka chemicals. Acid blue 25 (AB25; 45%), Methylene blue (MB; 70%), Aniline (C₆H₇N, 98 %), hydrochloric acid, Sulphuric acid, and sodium hydroxide were all supplied from Sigma-Aldrich company. Ammonium persulfate (APS; 98%), Disodium hydrogen phosphate (Na₂HPO₄, 99%), sodium dihydrogen phosphate (NaH₂PO₄, 98%), Ammonia (NH₃, 25%), and Ethanol (C₂H₆O, 95%) were obtained from Fisher company. All chemicals were used as received without further

purification and the double distilled water was used for all experiments.

Synthesis of In₂O₃ nanoparticles

Indium (III) oxide nanoparticles were prepared by the sol-gel procedure (Kulkarni and Patil 2016). Indium (III) nitrate hydrate (In(NO₃)₃ · xH₂O) and ammonia hydroxide were used. Firstly, indium (III) nitrate hydrate (2.5 g) was dissolved in water (60 mL) and subjected to sonication for 10 min where it ionizes in water. Secondly, the ammonia hydroxide solution (0.4 M) was added dropwise into the Indium (III) nitrate solution until the pH reached 9 and the mixture was stirred for 1 h. The obtained jelly material (In(OH)₃) was centrifuged for 30 min and washed thoroughly with water and then with ethanol to get rid of the excess ammonia. The gel was dried on a hot plate for 1 h at 100 °C and calcined for 1 h at 400 °C. After calcination, the white indium hydroxide, In(OH)₃, has converted into a yellowish-colored product of In₂O₃. The In₂O₃ was crushed by mortar to get the In₂O₃ nano-crystalline powder, Scheme (1).

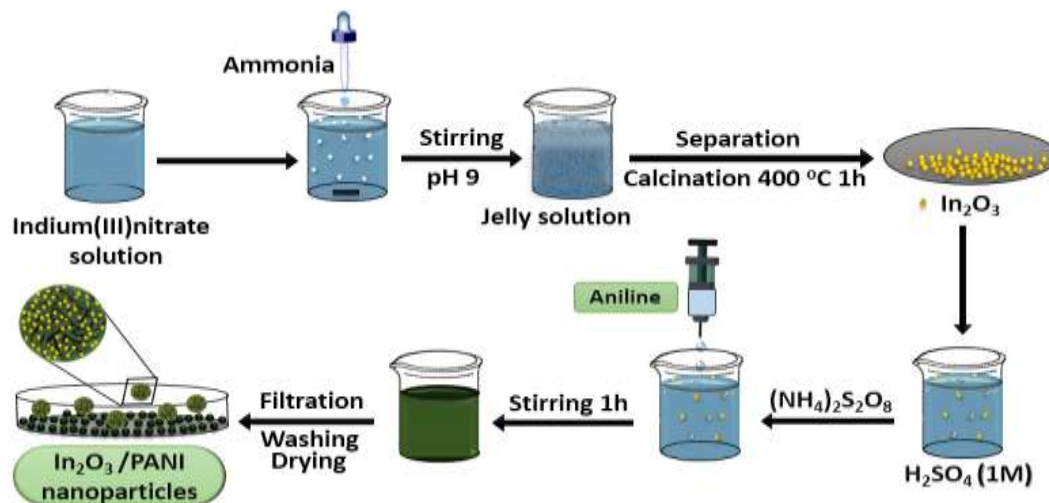
Polyaniline synthesis

Polyaniline (PANI) was synthesized via aniline polymerization in the presence of sulfuric acid (Salem, 2010). In brief, 7.5 g (0.033 mol) of (NH₄)₂S₂O₈ (APS) were

added to 200 mL of H₂SO₄ solution (1M) and magnetically stirred. Aniline (3 mL, 0.033 mol) was slowly added with stirring for 5 h to complete the polymerization process of aniline. The resulting polyaniline nanoparticles were filtered and thoroughly washed with H₂SO₄ solution (1M) followed by water until the filtrate became transparent. The polyaniline was dried at 60 °C for 24 h and ground.

Synthesis of In₂O₃/PANI nanocomposite

In₂O₃ (0.3 g) was transferred into 200 mL of H₂SO₄ solution (1M) and magnetically stirred. Following the addition of the APS (7.5 g, 0.033 mol) to the mixture, aniline (3 mL, 0.033 mol) was slowly added to the mixture. The polymerization reaction was then continued for 5 h with continual stirring. Filtration was used to separate the dark green precipitate, which was then repeatedly rinsed with H₂SO₄ solution (1M) until the filtrate attained colorless. Once the product was washed with water to remove any remaining acid, it was dried in an oven at 60 °C and ground, Scheme (1) (Akhter, Miran et al., 2012, Janeoo, Sharma et al., 2016, Salem, Elsharkawy et al., 2016).



Scheme (1) Preparation of In₂O₃ and In₂O₃/PANI nanocomposite by sol-gel and chemical oxidative polymerization method, respectively

Characterization

The synthesized In₂O₃/PANI nanocomposite was inspected by FT-IR (Shimadzu-8400S, Japan), while the spectra were investigated in the region of 4000-400 cm⁻¹. X-ray diffractometer (XRD; GNR, APD 2000 PRO model) was used to investigate the crystal phases. A scanning electron microscope (SEM, JSM-6510LV, Tokyo, Japan) and a transmission electron microscope (TEM, JEM-2100 plus, JEOL, Tokyo, Japan) were used to analyze the surface morphology of an In₂O₃/PANI nanocomposite. The elemental analysis of In₂O₃/PANI nanocomposite was carried out by the SEM device with Energy Dispersive X-ray (EDX) analysis. Furthermore, the surface area of the as-fabricated adsorbent was estimated by the BET method and the surface charge of the nanocomposite was determined by

the zeta potential (Malvern Zetasizer Nano series, (UK).

Adsorption study

The AB25 adsorption onto the In₂O₃/PANI nanocomposite was carried out into several conical flasks (100 mL) containing a definite quantity of In₂O₃/PANI (0.007 g), water (17 mL), and 3 mL of AB25 solution (10⁻³ mol/L). Into a water shaker thermostat at 30 °C and 120 rpm, the flasks were mounted. The adsorption of the AB25 was commenced once a definite volume of AB25 solution was added. At regular time intervals, the flasks were sequentially removed from the thermostat and a sample of AB25 solution (3 mL) was transferred into a 1-cm quartz cell and the absorbance was measured at $\lambda_{\text{max}} = 605$ nm. The removal percentage was then calculated from Equ (1). The amount of AB25 adsorbed at time *t* and the equilibrium was also

determined from Eqs. (2) and (3), respectively.

$$\text{Removal efficiency \%} = \frac{(C_o - C_t)}{C_t} \times 100 \quad (1)$$

$$q_t = \frac{(C_o - C_t)}{m} \times V \quad (2)$$

$$q_e = \frac{(C_o - C_e)}{m} \times V \quad (3)$$

The amounts of AB25 adsorbed at time t and at equilibrium are represented by q_t and q_e (mg/g), C_o and C_t (mg/L) represent the initial and time-dependent concentrations of AB25 in solution, respectively. C_e (mg/L) is the concentration of AB25 in solution at equilibrium. m (g) is the mass of the nanocomposite, and V (L) is the operating volume of the dye solution.

Results and Discussion

Characterization of adsorbent

FT-IR

The FT-IR spectra of In_2O_3 , PANI, and $\text{In}_2\text{O}_3/\text{PANI}$ were captured in the 4000-400 cm^{-1} region and are shown in Fig (1a). In the case of In_2O_3 , the typical peaks of In_2O_3 are present at 536, 560, and 597 cm^{-1} and are attributed to the stretching vibration of the In-O bonds, while the peaks at 877 and 1329 cm^{-1} are attributed to the bending vibration of the In-O-In. Hydrogen bond stretching vibrations are responsible for the absorption peak at 3472 cm^{-1} (Sridhar B, Husain et al., 2016, Pan, Qian et al., 2021). For PANI, the peak around 661

cm^{-1} is typical of C-C. The in-plane and out-of-plane C-H bonds produced peaks at 852 and 727 cm^{-1} , respectively. The C=C and C=N stretching vibrations of the benzenoid and quinoid rings are respectively characterized by the peaks at 1480 and 1538 cm^{-1} . The peaks at 1209 and 1383 cm^{-1} are characteristic of the stretching vibration of C-N in the benzenoid structure; the quinoid structure shows the peak at 1078 cm^{-1} . Furthermore, the broad peak at 3236 cm^{-1} is assigned to the N-H stretching vibrations. In the case of $\text{In}_2\text{O}_3/\text{PANI}$ nanocomposite, the existence of a new peak at 559 cm^{-1} proves the presence of In_2O_3 in the PANI matrix. The peaks of 856 and 682 cm^{-1} are primarily assigned to the in-plane and out-of-plane C-H bonds, respectively. The peaks at 1428 and 1537 cm^{-1} are due to the C=C and C=N stretching vibrations of benzenoid and quinoid rings, respectively. The peaks at 1208 and 1280 cm^{-1} are due to the C-N stretching vibration of the benzenoid unit while the peak at 1079 cm^{-1} is assigned to the stretching vibration of the quinoid unit. The broad peak at 3268 cm^{-1} is assigned to the stretching vibrations of the N-H bond. According to Fig. (1a), it is seen that the $\text{In}_2\text{O}_3/\text{PANI}$ peaks are quite small with a slight shift in the wavenumber. This shift means the presence of In_2O_3 in the PANI matrix and there is an interaction

between In₂O₃ and PANI. The presence of the broad peak of the N–H bond confirms the physical interactions between In₂O₃ and PANI by van der Waals attraction forces (Janeoo, Sharma et al. 2016, Abd Ali, Ismail et al. 2021).

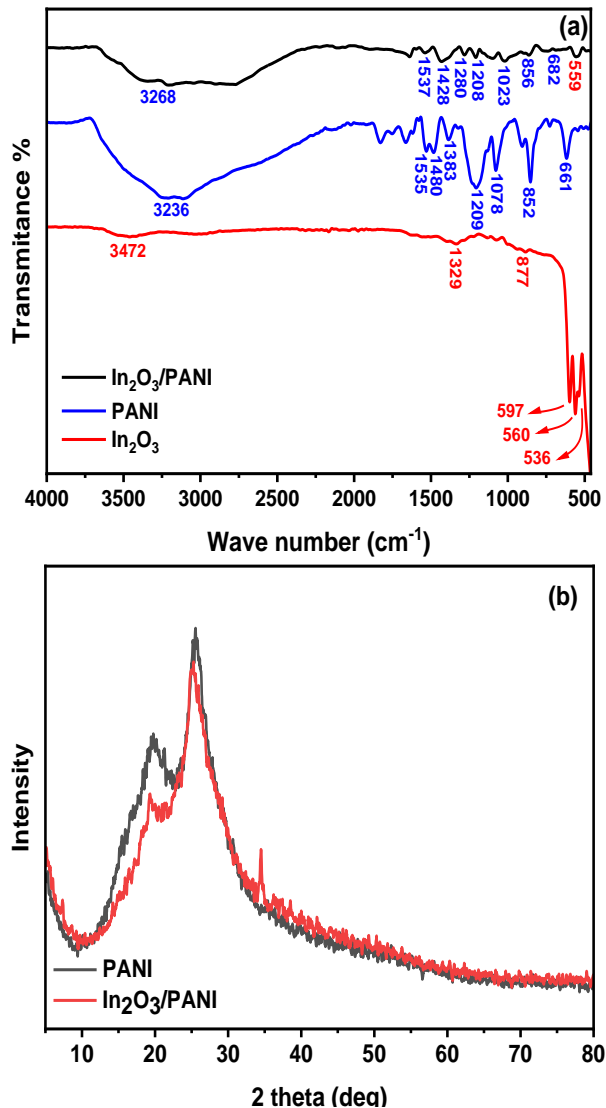


Fig. (1): (a) FT-IR spectra of In₂O₃, PANI and In₂O₃/PANI, (b) XRD patterns of In₂O₃/PANI

XRD

Fig. (1b) illustrates that the In₂O₃/PANI nanocomposite has an amorphous structure with a broad peak observed at 25.3° on the crystal plane (222). It is depicted that the XRD of the

nanocomposite is similar to that of PANI, indicating that the molecular chain structure of PANI wasn't destroyed. It is also noticed that the new peak appearing at 34.39° is corresponding to the (400) plane. This confirms the inclusion of In₂O₃ nanoparticles into the PANI matrix (Benykhlef, Bekhoukh et al., 2016, Janeoo, Sharma et al., 2016, Sridhar B, Husain et al., 2016.).

SEM and EDX

The SEM images of In₂O₃, PANI, and In₂O₃/PANI are displayed in **Fig. (2 a-c)**. The In₂O₃ nanoparticles are spherical and have nanoscale dimensions with uniform dispersion. The micrograph also displays the distribution of the spherical In₂O₃ nanoparticles homogeneously on the PANI surface. These observations indicate that the present nanocomposite may have a good adsorption capacity (Jebreil 2014, Tanzifi 2016). The EDX analysis was used to determine the chemical structure of the nanocomposite. It depicts the existence of C, N, O, and In, whose weight percentages are listed in Table (1).

Table (1): EDX analysis of In₂O₃/ PANI nanocomposite

Elements	Weight %
C	90.79
N	5.69
O	1.02
In	2.50

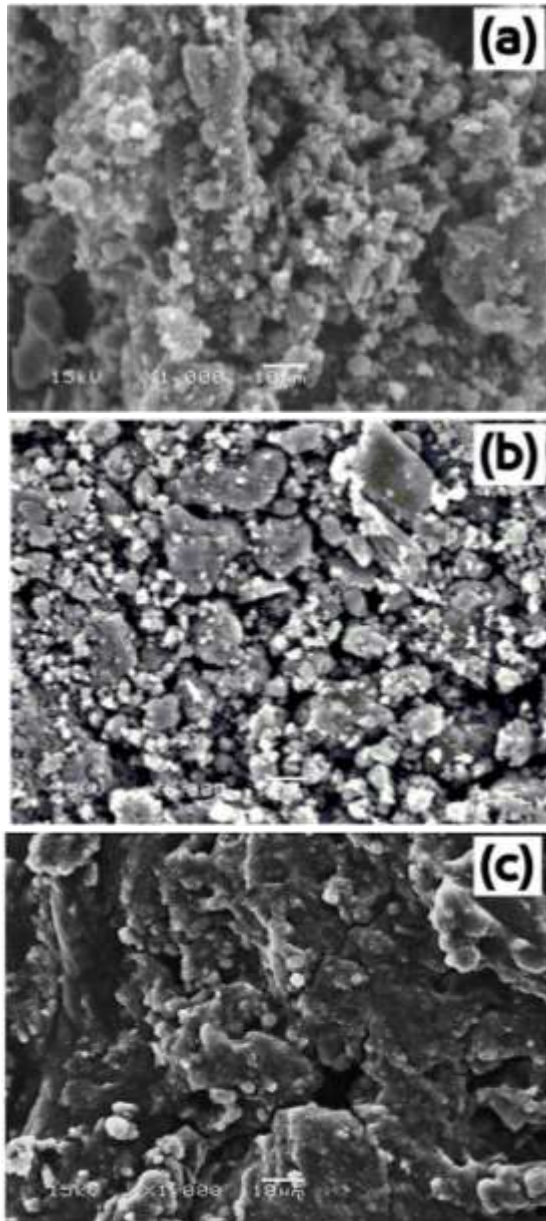


Fig. (2): SEM image of (a) In₂O₃, (b) PANI, (c) In₂O₃/PANI nanocomposite

TEM

The In₂O₃ and In₂O₃/PANI TEM images are displayed in **Fig. (3)**. The In₂O₃ nanoparticles are almost spherical with nearly homogeneous distribution **Fig. (3a)**. The particle size of In₂O₃ varies from 7.47 to 12.54 nm (**Kulkarni and Patil 2016**). **Fig. (3b)** shows the TEM nanocomposite with an average diameter of 58.43 nm.

micrograph of In₂O₃/PANI

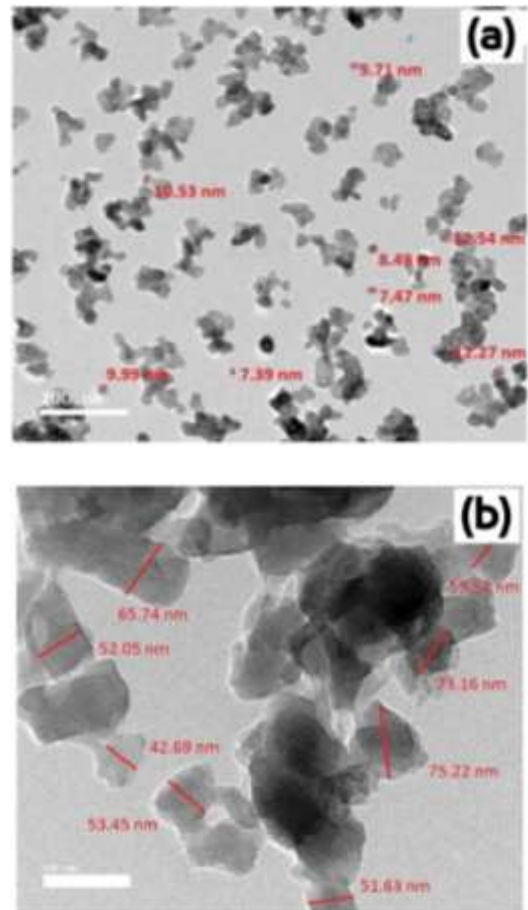


Fig. (3): TEM image of (a) In₂O₃ and (b) In₂O₃/PANI nanocomposite

BET

The BET adsorption theory is the most well-known to measure the adsorbent surface area. In this study, the relative pressure (P/P^0) range between 0.55 and 1 was used to measure the specific surface area of the In₂O₃/PANI nanocomposite.

Fig. (4a) depicts the N₂ adsorption-desorption on the surface of the nanocomposite. The adsorption-desorption behavior belongs to the type-IV isotherm with a surface area of 46.92 m²/g, pore volume of 0.387 cm³/g, and average pore diameter of 98.565 nm. The bare PANI has a surface area of

31.901 m²/g, a pore volume of 0.2719 cm³/g, and a pore diameter of around 72.725 nm.

Zeta potential measurement

The point of zero-charge (pH_{zpc}) of the surface is considered a significant parameter that affects the mechanism of adsorption. In Fig. (4b), the pH_{zpc} of In₂O₃/PANI is 7.13. It means that the nanocomposite surface has positive charges at a solution pH lower than pH_{zpc}. In this case, the electrostatic interaction is strong between the nanocomposite surface and the anionic AB25 molecules. In contrast, at initial pH higher than pH_{zpc}, the nanocomposite surface attains negative charges that enhance the electrostatic repulsion between the nanocomposite surface and AB25 molecules. Consequently, the efficiency of AB25 removal decreases at high pH. Accordingly, the adsorption of AB25 becomes most favorable in acidic medium (Fuseini, El Shazly et al., 2020).

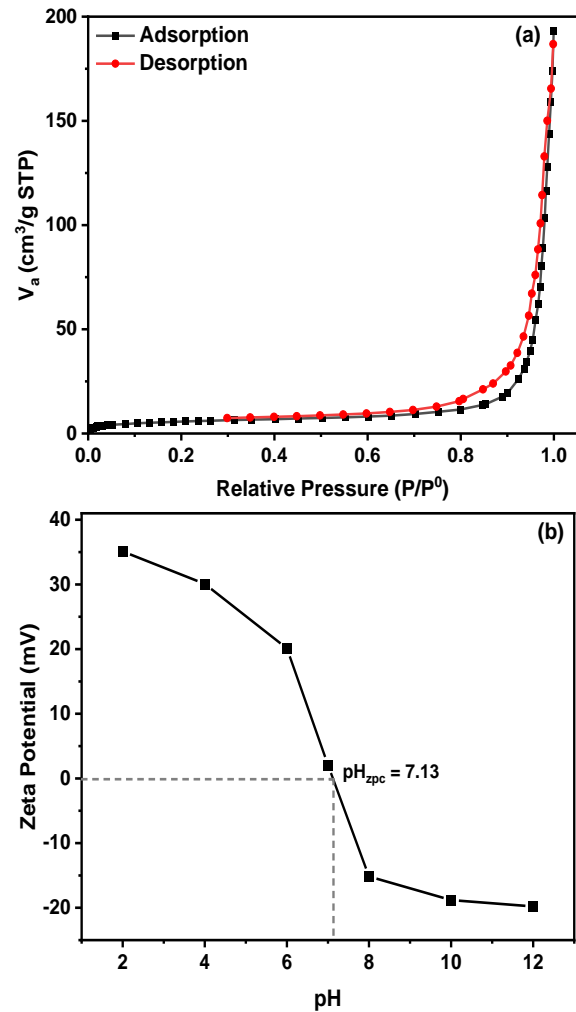


Fig. (4): (a) BET curve of In₂O₃/PANI nanocomposite, (b) Zeta potential analysis of In₂O₃/PANI nanocomposite at different pH

Kinetic and selectivity studies

In₂O₃, PANI, and In₂O₃/PANI were individually applied as adsorbents to remove the AB25 under the same conditions, [AB25]₀ = 48.09 mg/L, adsorbent dose = 0.007g at 30 °C. The removal efficiency obtained was 9, 25, and 95.5%, respectively. Since the In₂O₃/PANI has proved the most effective adsorbent than In₂O₃ and PANI, it was thus selected to remove the AB25 from the solution via adsorption under several conditions. The removal process was followed by monitoring with time

the decrease of dye absorbance at λ_{\max} 605 nm which was accompanied by the disappearance of color over time. Because the wastewater normally contains various dyes of different charges which may interact together, it was important to investigate the adsorption selectivity of each dye in the mixture solution (**El-Monaem, Eman et al., 2022**). The selectivity of $\text{In}_2\text{O}_3/\text{PANI}$ nanocomposite was examined for a single dye (methylene blue, MB) and a binary mixture of MB and AB25. In a typical experiment, $\text{In}_2\text{O}_3/\text{PANI}$ (0.007g) was added to 20 mL dyes solution at 30 °C. The initial concentration of both the MB and AB25 was 10 mg/L (**Bhattacharyya, Ghorai et al., 2021**). The removal percentage of the AB25 in a single form and a binary mixture with MB was 98% and 51.4% after 90 min, respectively. Furthermore, the removal percentage of single MB in a mixture with AB25 was 14 % and 33.9% after 90 min, respectively.

The dye selectivity in the mixture was estimated by the ratio of the two static distribution coefficients K_{D1} and K_{D2} for the AB25 and MB. This ratio is the separation factor (α) which is used to calculate the molecular selectivity of the nanocomposite. The high value of α denotes a better selectivity. If α is close to unity, then the adsorbent has no selectivity (**Mahmoodi, 2014**). The

parameters K_D and α were calculated by Eqs. (4) and (5). In this study, the static distribution coefficients were 3.02 and 1.47 mL/g for AB25 and MB, respectively. Therefore, the separation factors were 2.08 and 0.48 for AB25 and MB, respectively. From these results, it was found that AB25 is the more selective dye by the nanocomposite and therefore was chosen as a model pollutant for this study.

$$K_D = q_e / C_e \quad (4)$$

$$\alpha = K_{D2} / K_{D1} \quad (5)$$

Adsorption study by batch mode technique Effect of $\text{In}_2\text{O}_3/\text{PANI}$ dose

At a fixed concentration of AB25 (48.09 mg/L) and a variable dose of nanocomposite in the 0.005-0.02 g range, the effect of dose on AB25 adsorption was examined under the following condition: $[\text{AB25}]_0 = 48.09$ mg/L, agitation speed of 120 rpm and temperature 30°C in aqueous solutions. The dye removal percentage increased from 94.28% to 99.99% with the dose increase from 0.005 to 0.02 g, as shown in Fig. (5a). By increasing the dose, the number of active sites on the nanocomposite surface available for adsorption of AB25 molecules increases and consequently the removal percentage increases (**TaheriAshtiani and Ayati, 2022**). The removal efficiency reached 99.99 % at a dose of

0.0125 g of the nanocomposite. This is explained by the high availability of the adsorption sites on the In₂O₃/PANI surface, which resulted from an increase in the dosage of the nanocomposite with a constant concentration of AB25 in the bulk solution (El-Sawy, Gemeay et al., 2021). Based on the experimental results, a dose of 0.007 g was thus selected as the most appropriate amount of In₂O₃/PANI to explore the impacts of various variables on the adsorption process of AB25.

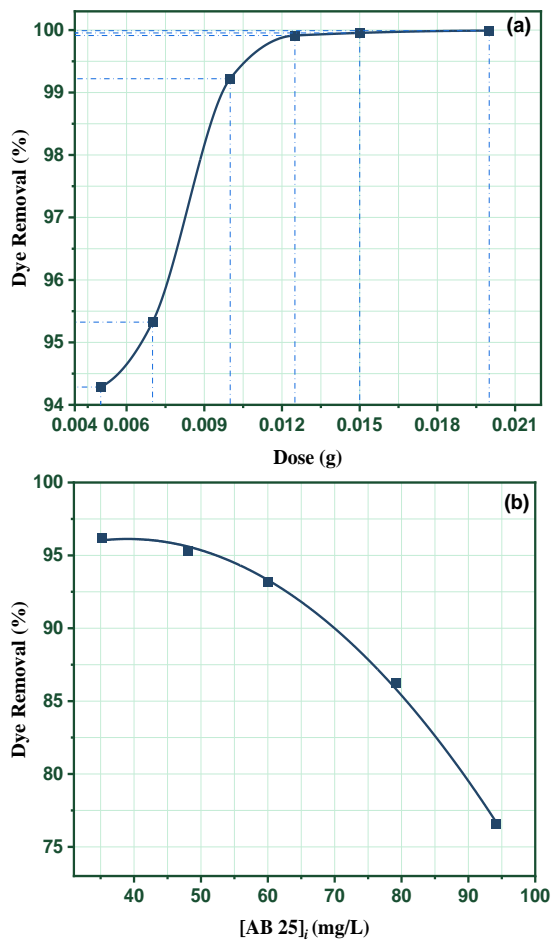


Fig. (5): (a) Effect of In₂O₃/PANI dose on the removal of AB25. [AB25]_o = 48.09 mg/L at 30 °C, (b) Effect of initial concentration of AB25 on the removal process. In₂O₃/PANI = 0.007 g at 30 °C

Effect of [AB25]_o

Under neutral pH, temperature of 30 °C, and agitation speed of 120 rpm, the impact of AB25 concentration on the removal percentage was investigated by maintaining the dose of In₂O₃/PANI constant at 0.007 g and varying the concentration of the dye from 35.27 to 94.1 mg/L. **Fig. (5b)** shows that as the concentration of AB25 falls, the removal percentage rises. The majority of the AB25 molecules that migrate from the bulk solution to the surface at low concentrations of AB25 are received and accommodated by the numerous active sites that are present on the In₂O₃/PANI surface. The adsorption process was therefore rapid and achieved high removal efficiency. In contrast, at a high concentration of AB25, the limited number of active sites due to the fixed dose of nanocomposite get occupied with AB25 molecules leaving behind the rest of the AB25 molecules in the solution. Adsorption of these free AB25 molecules on the unoccupied active sites becomes lower and lower with the continuous coverage of the available sites on the surface. As a result, AB25 is removed at a lower rate (Sarojini, Babu et al., 2022). These findings led to 48.09 mg/L being chosen as the initial concentration of AB25.

Effect of temperature

The temperature is well known to have a significant influence on the dye removal rate. To study this effect, the adsorption process was carried out at varied temperatures between 298 and 318 K, while other reaction conditions remained constant, including $[AB25]_0 = 48.09$ mg/L, $In_2O_3/PANI = 0.007$ g, and stirring rate of 120 rpm. Inspection of Fig. (6a) shows an increase in the removal percentage of AB25 from 94.81 to 99% when the temperature rose from 298 to 318 K (Salem, Elsharkawy et al., 2019). The primary cause of this phenomenon is the increase in the mobility of AB25 molecules towards the $In_2O_3/PANI$ surface with temperature. This demonstrates that AB25 adsorption on $In_2O_3/PANI$ is endothermic.

Thermodynamic parameters

The thermodynamic parameters give details on how the energies involved in the adsorption process fluctuate. Values of ΔH° and ΔS° determined from Fig. (6b) are reported in Table (4). The negative ΔG° indicate the spontaneity and feasibility of AB25 adsorption onto $In_2O_3/PANI$, while the endothermic nature of dye adsorption is confirmed by the positive value of ΔH° . The increased unpredictability of the solid/solution

interface is indicated by the positive value of ΔS° (Tka and Jabli et al., 2018).

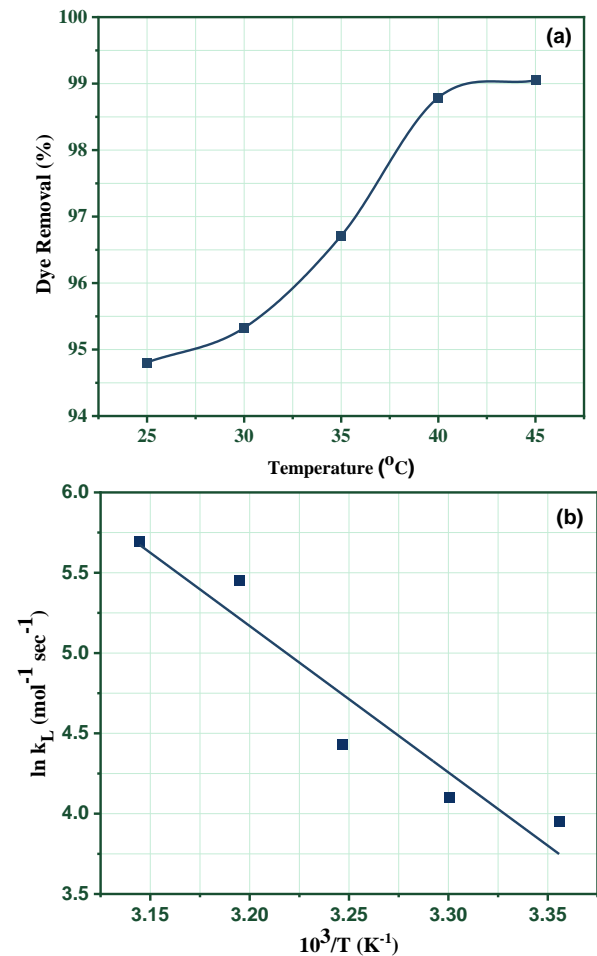


Fig. (6): (a) Effect of temperature on the removal of AB25. $[AB25]_i = 48.09$ mg/L, $In_2O_3/PANI = 0.007$ g, (b) Vand's Hoff plot

Table (2): Thermodynamic parameters for AB25 adsorption onto In₂O₃/ PANI

Equation	Parameter	Temperature (K)				
		298	303	308	313	318
$\ln\left(\frac{q_e}{C_e}\right) = \frac{\Delta S^\circ}{R} - \frac{\Delta H^\circ}{RT}$	K_L (L/g)	52.142	60.604	83.984	232.857	297.142
$K_L = \frac{q_e}{C_e}$	ΔG° (kJ/mol)	-9.796	-10.339	-11.345	-14.183	-15.054
	ΔH° (kJ/mol)	75.807				
$\Delta G^\circ = \Delta H^\circ - T(\Delta S^\circ)$	ΔS° (J/K.mol)	285.554				

Effect of pH

The adsorption of AB25 onto In₂O₃/PANI nanocomposite was found to be affected by the pH of the solution. It is known that the initial pH influences the charge of the nanocomposite surface (Tka and Jabli et al., 2018) and the chemistry of the dye in solution. The adsorption of AB25 was followed in solutions having pH from 2 to 12, [AB25]_i = 48.09 mg/L, In₂O₃/PANI = 0.007 g, and stirring speed of 120 rpm at 30 °C. The removal percentage of AB25 decreased from 99.91 to 48.75 % as the pH was increased from 2 to 12. Fig. (7) illustrates the relationship between pH change and removal percentage. The removal percentage is high at a lower pH range. At lower pH, the [H⁺] in solution is high and may protonate the amine centers of the PANI skeletal in the In₂O₃/PANI nanocomposite and therefore enhancing the electrostatic attraction of the surface with the AB25 molecules. With increasing the pH, the

number of AB25 molecules adsorbed onto the surface decreases owing to the decrease in the electrostatic attraction between the In₂O₃/PANI surface and the AB25 molecules. In the basic medium, less positive active sites are present on the nanocomposite surface. As a result, there is the less electrostatic interaction between the AB25 and In₂O₃/PANI surface. This decreases the dye removal percentage (Hanafiah and Ngah et al., 2012, Jabli 2020). These results are supported by the results obtained from zeta potential analysis.

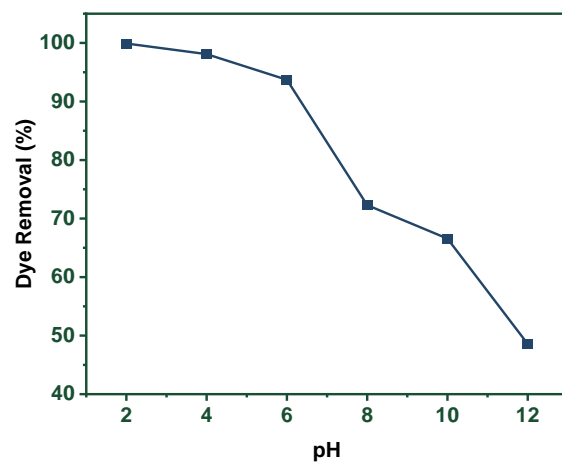


Fig. (7): Effect of pH on the adsorption of AB25 onto In₂O₃/PANI. [AB25]_i = 48.09 mg/L, In₂O₃/PANI = 0.007 g at 30 °C

Adsorption kinetics

Two models of adsorption kinetics were applied for the adsorption of AB25 by $\text{In}_2\text{O}_3/\text{PANI}$ and the results are summarized in Table (3). Inspection of these findings demonstrates that the model of pseudo-second-order kinetic is the most effective at present absorption process owing to its high value of correlation coefficient ($R^2=0.999$), Fig. (8a).

To confirm the diffusion mechanism, the Weber-Morris intraparticle diffusion model was also applied to the adsorption procedure. As shown in Fig. (8b), the adsorption process consists of three adsorption steps. In the first step, the AB25 molecules diffuse from the bulk solution and are adsorbed onto the surface of $\text{In}_2\text{O}_3/\text{PANI}$. The second stage explains the diffusion of the AB25 molecules from the exterior surface into the internal voids of the $\text{In}_2\text{O}_3/\text{PANI}$ nanoparticles. At high concentrations of AB25, the third stage indicating the equilibrium state of the adsorption is observed. The dye molecules migrate from the big holes to the micro pores in the nanocomposite surface during the

Adsorption isotherms

Adsorption isotherm models are useful for determining the maximum amount of adsorbate that may be absorbed by a given amount of adsorbent and for characterizing how the adsorbate and

third stage, which is characterized by a slow adsorption rate. This is accomplished by saturating the active sites with the dye molecules (El-Ghobashy and Hashim et al., 2022). The kinetic data of this model are summarized in Table (5).

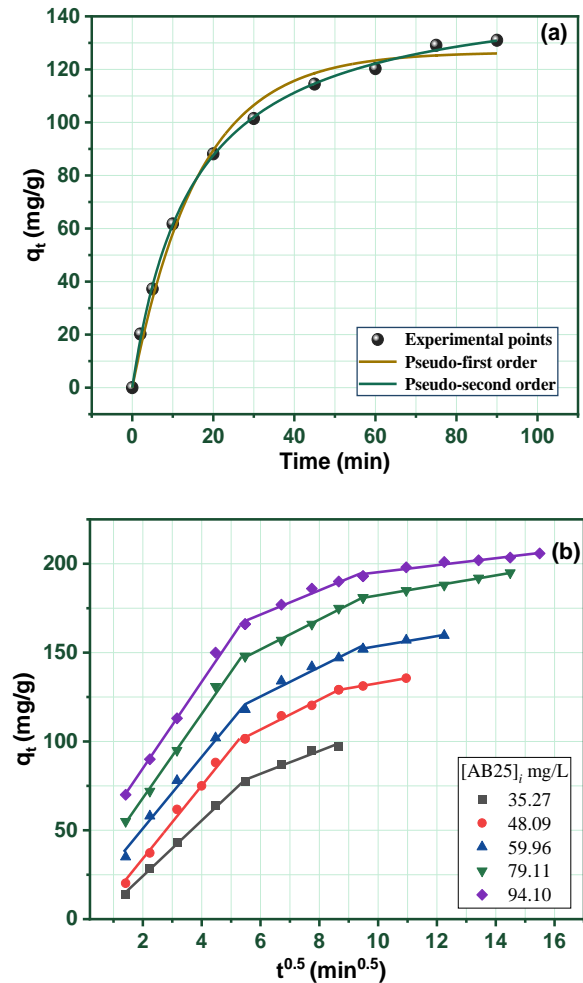


Fig. (8): (a) Adsorption Kinetic models of AB25 on $\text{In}_2\text{O}_3/\text{PANI}$ nanocomposite. $[\text{AB25}]_i = 48.09$ mg/L, $\text{In}_2\text{O}_3/\text{PANI} = 0.007$ g at 30°C , (b) Intraparticle diffusion model of AB25 on $\text{In}_2\text{O}_3/\text{PANI}$ nanocomposite. $\text{In}_2\text{O}_3/\text{PANI} = 0.007$ g at 30°C

adsorbent interact (Shah and Rahman et al., 2019). As a result, the adsorption data for AB25 on the $\text{In}_2\text{O}_3/\text{PANI}$ nanocomposite were introduced to the Langmuir, Freundlich, Temkin, Redlich-

Peterson, and Toth models. These models are divided into two categories.

Table (3): Adsorption kinetic data for the adsorption of AB25 onto In₂O₃/ PANI

Kinetic model	Parameter	Initial concentration of AB25 (mg/L)				
		35.27	48.09	59.96	79.11	94.10
Pseudo-first-order $q_t = q_e(1 - e^{-k_1 t})$	$q_{e, \text{exp}}$ (mg/g)	96.95	131.22	159.66	194.99	205.82
	$q_{e, \text{cal}}$ (mg/g)	96.35	129.25	149.51	180.26	193.18
	k_1 (min ⁻¹)	0.056	0.058	0.067	0.074	0.097
	R^2	0.992	0.986	0.946	0.915	0.895
Pseudo-second-order $q_t = \frac{t k_2 q_e^2}{1 + t k_2 q_e}$	$q_{e, \text{exp}}$ (mg/g)	96.95	131.22	159.66	194.99	205.82
	$q_{e, \text{cal}}$ (mg/g)	120.35	152.42	168.95	198.05	207.45
	$k_2/10^4$ (g/mg. min)	4.43	4.87	5.27	5.33	7.19
	R^2	0.999	0.999	0.987	0.977	0.973
Intraparticle Diffusion $q_t = k_p t^{0.5} + c$	kp_1 (mg/g min ^{1/2})	15.61	20.5	20.128	23.70	24.34
	R^2	0.998	0.99	0.990	0.995	0.997
	kp_2 (mg/g min ^{1/2})	6.42	6.25	8.25	8.407	6.82
	R^2	0.955	0.94	0.962	0.999	0.967
	kp_3 (mg/g min ^{1/2})	-	0.998	0.98	0.997	1.97
	R^2	-	2.87	2.79	2.80	0.956

The first category involves the two-parameter models like Langmuir, Freundlich, and Temkin. The second is the three-parameter models like Redlich-Peterson and Toth (**Islam and Ali et al., 2019**). Table (4) lists the equations and parameter values for these isotherm models (**Ghanei and Rashidi et al., 2018**). The equilibrium data were evaluated by using different initial concentrations of AB25 from 35.27 to 94.1 mg/L at the fixed amount of In₂O₃/PANI (0.007 g) and constant temperature of 30 °C. The nonlinear connection between q_e and c_e for all these models is depicted in Fig. (9), but all the parameters of these models were determined according to the linear equations (not shown).

Langmuir isotherm

According to this isotherm, adsorption occurs at specific homogenous surfaces via the formation of a monolayer with no chemical interaction between the adsorbate molecules that adsorbed on active sites having constant adsorption energy (**Salem and Salem et al., 2017**). The advantage of the isotherm is recognized from a dimensionless separation factor (R_L), as given by Equ (6) (**Tanzifi, 2016**).

$$R_L = \frac{1}{1 + K_L c_i} \quad (6)$$

The adsorption state can be predicted based on the R_L value. The adsorption is favorable at $0 < R_L < 1$, unfavorable at $R_L > 1$, linear at $R_L = 1$, and irreversible at $R_L = 0$. Since the current R_L value (0.0336) falls between 0 and 1, the

adsorption of AB25 on the $\text{In}_2\text{O}_3/\text{PANI}$ surface is favorable. The high value of R^2 indicates that the adsorption occurs on the uniform active sites of the surface (Kareem and Abd Alrazak et al., 2016), Table (4).

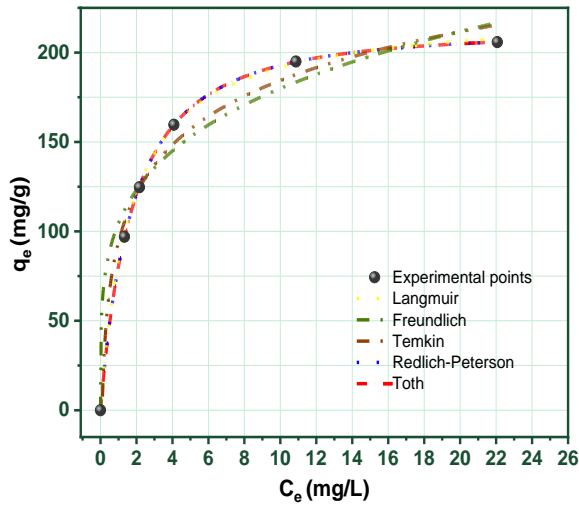


Fig. (9): Non-linear adsorption isotherm models for the removal of AB25 onto $\text{In}_2\text{O}_3/\text{PANI}$ nanocomposite

Table (4): Non-linear data of adsorption isotherm models for adsorption of AB25 onto $\text{In}_2\text{O}_3/\text{PANI}$

Isotherm	Equation	Parameter	Value
Langmuir	$q_e = \frac{q_m K_L C_e}{1 + k_L C_e}$	q_m (mg/g)	223.61
		K_L (L/mg)	0.598
		R_L	0.0336
		R^2	0.9999
Freundlich	$q_e = K_F C_e^{1/n_F}$	$1/n_F$	0.235
		n_F	4.255
		K_F (mg/g ^{1/n_F}) (L/mg) ^{1/n_F}	104.614
		R^2	0.9767
Temkin	$q_e = B_T \ln K_T C_e$	K_T (L/mg)	10.986
		B_T (kJ/mol)	39.244
		R^2	0.9887
Redlich-Peterson	$q_e = \frac{K_R C_e}{1 + a_R C_e^{n_R}}$	K_R (L/mg)	118.712
		a_R (L/mg) ^{n_R}	0.473
		n_R	1.037
		R^2	0.9999
Toth	$q_e = \frac{q_m K_t C_e}{[1 + (k_t C_e)^t]^{1/t}}$	q_m (mg/g)	253.36
		K_T (L/mg)	0.486
		t	1.037
		R^2	0.9999

Freundlich isotherm

The isotherm discusses the adsorption of a substance on a heterogeneous surface of varied heat of adsorption based on multilayer adsorption at unequal active sites (**Islam and Ali et al., 2019**). The constants of Freundlich isotherm n_F and K_F are used to determine the heterogeneity of the nanocomposite. If n_F is less than 1, it refers that adsorption is chemical while at $n_F > 1$ it is physical adsorption with a homogeneous active site distribution. The greater the K_F value, the greater the nanocomposite's maximum capacity (**El-Ghobashy, Hashim et al., 2022**). Since the $1/n_F = 0.235$, $n_F = 4.25$, and $K_F = 104.62$, they indicate favorable physical adsorption of AB25 onto the In₂O₃/PANI with homogeneous active sites distribution, Table (4).

Temkin isotherm

This isotherm demonstrates that the adsorption heat generated by the adsorbate molecules within the layer decreases linearly with the increase in surface coverage due to the interaction between the adsorbent and adsorbate. In addition, the consistent distribution of binding energies is another factor that distinguishes such adsorption. The heat of adsorption (b_T) and the Temkin isotherm constant (B_T) are related to each other as in Equ. (7).

$$B_T = \frac{R T}{b_T} \quad (7)$$

Since the B_T value (39.24 kJ/mol) given in Table (4) lies in the range 20-40 kJ/mol, then the adsorption of AB25 onto In₂O₃/PANI is physisorption.

Redlich-Peterson isotherm

In the Redlich-Peterson isotherm, the properties of the Freundlich and Langmuir adsorption isotherm models are combined. Therefore, it applies to both homogeneous and heterogeneous systems. The Redlich-Peterson model approaches the Freundlich isotherm at high concentrations as the n_R value tends to zero. It can also be applied as a Langmuir isotherm when the n_R is closer to one at low concentrations (**Nethaji and Sivasamy et al., 2013**). Since the value of n_R in Table (4) equals 1.037, it is very close to 1 and indicates that the Redlich-Peterson isotherm is described as the Langmuir isotherm with a uniform distribution of adsorption sites.

Toth isotherm

The basis for the Toth isotherm is the quasi-Gaussian energy distribution theory that has been developed to improve the Langmuir isotherm fittings. According to this paradigm, the adsorption takes place on particular homogenous surfaces by considering sub-monolayer coverage. If the dimensionless parameter (t) is closer to 1, the Toth model changes into the

Langmuir isotherm model. Table (4) displays the nonlinear equation and the parameters of this isotherm. The value of t and R^2 derived from Fig. (9) are 1.037 and 0.999. Thus, the current adsorption process is fitted well with this model that considers the adsorption of AB25 at a homogeneous surface (Janaki and Vijayaraghavan et al., 2012).

Based on the correlation coefficients (R^2) values, the experimental data were found to be consistent with the Langmuir, Redlich-Peterson, and Toth isotherm models, demonstrating that the adsorption of AB25 onto the $\text{In}_2\text{O}_3/\text{PANI}$ proceeds through a sub-monolayer attachment and the active sites are uniform. Further, the isotherm constants confirmed that the $\text{In}_2\text{O}_3/\text{PANI}$ surface was homogenous and the adsorption was a favorable physical process. Table (4) provides the derived parameters values and correlation coefficients (R^2) for each isotherm.

Reusability of the nanocomposite

The nanocomposite reusability study is important to ascertain its stability and feasibility for application. The $\text{In}_2\text{O}_3/\text{PANI}$ nanocomposite was collected after each adsorption run. Since the nanocomposite exhibited high adsorption efficiency under strongly acidic conditions, it was thus rinsed in NaOH solution (0.1 M) for 12 h. In this

basic medium, the adsorption sites acquire negative charges which repel the adsorbed anionic dye molecules through an electrostatic attraction. Such repulsion has forced the dye molecules to desorb from the nano surface into the solution. The nanocomposite was then collected by filtration, rinsed with water many times, and then dried at 60 °C in an oven for 12 h (Janaki, Vijayaraghavan et al. 2012). Five cycles of the adsorption-desorption process were carried out under the same conditions and the results obtained are illustrated in Fig. (10). The removal percentage of AB25 has slightly decreased from 95.5 to 83 % after the fifth cycle, suggesting high stability of the nanocomposite. Therefore, it can be considered a good recyclable adsorbent for application in the treatment of wastewater.

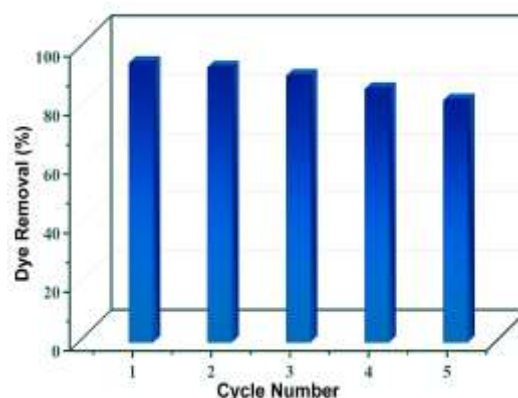


Fig. (10): Reusability of $\text{In}_2\text{O}_3/\text{PANI}$ nanocomposite for AB25 dye removal. $[\text{AB25}]_i = 48.09 \text{ mg/L}$, $\text{In}_2\text{O}_3/\text{PANI} = 0.007 \text{ g}$ at 30 °C

Comparative study

Table (5) shows the highest adsorption capacity (q_{max}) of $\text{In}_2\text{O}_3/\text{PANI}$ for the

removal of AB25 compared with some of the other adsorbents. The present q_{\max} is 223.61 mg/g at a removal percentage of 95.5 %. Although the adsorption was carried out in a weakly acidic medium (pH=6.2), the In₂O₃/PANI nanocomposite showed better removal

efficiency than other adsorbents (Hanafiah and Ngah et al., 2012; Tka and Jabli et al., 2018, Krishna, Soontarapa et al., 2019; Jain, Tamboli et al., 2020; Chaudhary and Singh et al., 2021; Lakkaboyana and Soontarapa et al., 2021).

Table (5): Comparison of the maximum adsorption capacities for the removal of AB25

Adsorbent	pH	T (°C)	q_{\max} (mg/g)	Reference
Ethylene diamine-fiber	4	60	67	Tka, Jabli et al., 2018
Base treated shorea dasyphylla	2	27	24.39	Hanafiah, Ngah et al., 2012
Waste tea residue	1	45	127.14	Jain, Tamboli et al., 2020
Chitosan/PVA @CuO	5	40	171.4	Lakkaboyana, Soontarapa et al., 2021
Activated carbon	6	25	209	Chaudhary, Singh et al., 2021
Zeolite-CTAB	2	60	112.44	Krishna, Soontarapa et al., 2019
In ₂ O ₃ /PANI	6.2	30	223.61	Present study

Conclusion

The In₂O₃/PANI nanocomposite was successfully synthesized and characterized. The nanocomposite particles have an average diameter of 58.43 nm, a surface area of 46.92 m²/g, and a pore volume of 0.387 cm³/g. The effective impregnation of In₂O₃ nanoparticles into the PANI matrix was confirmed by the EDX examination results, which indicated the coexistence of C, N, O, and In. Compared with the individual components, the developed In₂O₃/PANI nanocomposite showed better adsorption performance. The nanocomposite adsorbed the AB25 dye more efficiently than the cationic MB dye, proving its better selectivity

towards anionic dyes. Moreover, the adsorption of the AB25 also conformed to the pseudo-second-order kinetic model and matched the Langmuir and Toth isotherm models. The thermodynamic analysis demonstrated the spontaneous and endothermic nature of the adsorption process, whereas the Toth isotherm model revealed maximum adsorption capacity of 253.36 mg/g. A high recycling competency of the nanocomposite was noticed over five adsorption-desorption cycles with a removal efficiency reaching 83 %. Therefore, the enhanced adsorption capacity and the potential for reusability highlighted the fact that In₂O₃/PANI nanocomposite may be used successfully

to remove anionic dyes from aquatic systems.

Funding

No funding of any kind has been provided for this study.

Declaration of Competing Interest

The authors have no declared competing interests that are pertinent to the subject matter of this article.

References

- Abd Ali, L., H. K. Ismail, H. F. Alesary and H. Aboul-Enein (2021). "A nanocomposite based on polyaniline, nickel and manganese oxides for dye removal from aqueous solutions." *Int. J. Environ. Sci. Tech.*, **18**(7): 2031-2050.
- Akhter, U., M. Miran, M. Susan, M. Mollah and M. Rahman (2012). "Preparation and characterization of polyaniline-silica composite material." *Bangladesh J.Sci. Ind. Res.* **47**(3): 249-256.
- Al-Musawi, T. J., P. Rajiv, N. Mengelizadeh, I. A. Mohammed and D. Balarak (2021). "Development of sonophotocatalytic process for degradation of acid orange 7 dye by using titanium dioxide nanoparticles/graphene oxide nanocomposite as a catalyst." *J. Environ. Manag.*, **292**: 112777.
- Ali, I., T. Kon'kova, E. Liberman, E. Simakina, Z. A. ALOthman, T. S. Alomar and M. A. Islam (2022). "Preparation and characterization of SnO₂-CeO₂ nanocomposites: Sorption, modeling and kinetics for azorubine dye removal in water." *J. Mol. Liq.* **346**: 117119.
- Ayad, M. M., A. A. El-Nasr and J. Stejskal (2012). "Kinetics and isotherm studies of methylene blue adsorption onto polyaniline nanotubes base/silica composite." *J. Ind. Eng. Chem.* **18**(6): 1964-1969.
- Ayoub, Z. A., O. A. Yazbeck and M. M. el jamal (2017). "kinetic study of acid blue 1 discoloration with persulfate." *J. Chem. Tech. Metall* **52**(5).
- Bagheri-Mohagheghi, M. M., N. Shahtahmasebi, E. Mozafari and M. Shokooh-Saremi (2009). "Effect of the synthesis route on the structural properties and shape of the indium oxide (In₂O₃) nano-particles." *Phys. E: Low- Dimens. Syst.Nanostruct.* **41**(10): 1757-1762.
- Benykhlef, S., A. Bekhoukh, R. Berenguer, A. Benyoucef and E. Morallon (2016). "PANI-derived polymer/Al₂O₃ nanocomposites: synthesis, characterization, and electrochemical studies." *Colloid. Polym. Sci.* **294**(12): 1877-1885.
- Bhattacharyya, A., S. Ghorai, D. Rana, I. Roy, G. Sarkar, N. R. Saha, J. T. Orasugh, S. De, S. Sadhukhan and D. Chattopadhyay (2021). "Design of an efficient and selective adsorbent of cationic dye through activated carbon-grapheneoxide nanocomposite: Study on mechanism and synergy." *Mater. Sci. Phy.* **260**: 124090.
- Chaudhary, M., R. Singh, I. Tyagi, J. Ahmed, S. Chaudhary and S. Kushwaha (2021). "Microporous activated carbon as adsorbent for the removal of noxious anthraquinone acid dyes: Role of adsorbate functionalization." *J. Environ. Chem. Eng.* **9**(5): 106308.
- Dalvand, A., E. Gholibegloo, M. R. Ganjali, N. Golchinpoor, M. Khazaei, H. Kamani, S. S. Hosseini and A. H. Mahvi (2016). "Comparison of Moringa stenopetala seed extract as a clean coagulant with Alum and Moringa stenopetala-Alum hybrid coagulant to remove direct dye from Textile Wastewater." *Enviro. Sci. Pollut. Res.* **23**(16): 16396-16405.
- Daneshvar, E., M. S. Sohrabi, M. Kousha, A. Bhatnagar, B. Aliakbarian, A. Converti and A.-C. Norrström

- (2014). "Shrimp shell as an efficient bioadsorbent for Acid Blue 25 dye removal from aqueous solution." *J. Taiwan Inst. Chem. Eng.* **45**(6): 2926-2934.
- Dessie, Y., S. Tadesse and Y. Adimasu (2022)**. "Improving the performance of graphite anode in a Microbial Fuel Cell via PANI encapsulated α -MnO₂ composite modification for efficient power generation and methyl red removal." *Chem. Eng. J. Advan.* **10**: 100283.
- El-Ghobashy, M. A., H. Hashim, M. A. Darwish, M. U. Khandaker, A. Sulieman, N. Tamam, S. V. Trukhanov, A. V. Trukhanov and M. A. Salem (2022)**. "Eco-Friendly NiO/Polydopamine Nanocomposite for Efficient Removal of Dyes from Wastewater." *Nanomater.* **12**(7): 1103.
- El-Monaem, A., M. Eman, A. M. Omer, G. M. El-Subruiti, M. S. Mohy-Eldin and A. S. Eltaweil (2022)**. "Zero-valent iron supported-lemon derived biochar for ultra-fast adsorption of methylene blue." *Biomass Convers. Biorefin.*: 1-13.
- El-Sawy, A. M., A. H. Gemeay, A. S. Helal and M. A. Salem (2021)**. "Catalytic degradation of methylene blue in aqueous solution by H₂O₂ and SiO₂-NH₂-Cu (II)@ SiO₂ nanoparticles as catalyst." *J. Mol. Liq.*, **341**: 117422.
- Ferrag, C., M. Noroozifar, A. R. Modarresi-Alam and K. Kerman (2022)**. "Graphene oxide hydrogel electrolyte for improving the performance of electropolymerized polyaniline solar cells." *J. Power Sour.*, **542**: 231796.
- Fuseini, M., A. H. El Shazly and M. F. El-Kady (2020)**. Effects of Doping on Zeta Potential and pH of Polyaniline Colloidal Suspension. *Mater. Sci. Forum, Trans Tech Publ.*
- Gilja, V., I. Vrban, V. Mandić, M. Žic and Z. Hrnjak-Murgić (2018)**. "Preparation of a PANI/ZnO composite for efficient photocatalytic degradation of acid blue." *Polym.*, **10**(9): 940.
- Hanafiah, M. A. K. M., W. S. W. Ngah, S. H. Zolkafly, L. C. Teong and Z. A. A. Majid (2012)**. "Acid Blue 25 adsorption on base treated Shorea dasyphylla sawdust: Kinetic, isotherm, thermodynamic and spectroscopic analysis." *J. Environ. Sci.*, **24**(2): 261-268.
- Islam, M. A., I. Ali, S. A. Karim, M. S. H. Firoz, A.-N. Chowdhury, D. W. Morton and M. J. Angove (2019)**. "Removal of dye from polluted water using novel nano manganese oxide-based materials." *J. Water Process. Eng.*, **32**: 100911.
- Jabli, M. (2020)**. "Synthesis, characterization, and assessment of cationic and anionic dye adsorption performance of functionalized silica immobilized chitosan bio-polymer." *Int. J. Biol. Macromol.*, **153**: 305-316.
- Jain, S. N., S. R. Tamboli, D. S. Sutar, S. R. Jadhav, J. V. Marathe, A. A. Shaikh and A. A. Prajapati (2020)**. "Batch and continuous studies for adsorption of anionic dye onto waste tea residue: Kinetic, equilibrium, breakthrough and reusability studies." *J. Clean. Prod.*, **252**: 119778.
- Janaki, V., K. Vijayaraghavan, B.-T. Oh, K.-J. Lee, K. Muthuchelian, A. Ramasamy and S. Kamala-Kannan (2012)**. "Starch/polyaniline nanocomposite for enhanced removal of reactive dyes from synthetic effluent." *Carbohydr. Polym.*, **90**(4): 1437-1444.
- Janeoo, S., M. Sharma, G. Singh and J. Goswamy (2016)**. Structural and optical characterization of In₂O₃/PANI nanocomposite prepared by in-situ polymerization. AIP Conf. Proc, AIP Publishing LLC.
- Jebreil, S. A. (2014)**. "Removal of tartrazine dye from aqueous solutions by adsorption on the surface of

- polyaniline/iron oxide composite." *Int. Sch. Sci. Res., Innov* **8**: 1346-1351.
- Jiang, Z., T. Liu, X. Zhai and J. Liu (2021).** "Optimization Preparation of Indium Tin Oxide Nanoparticles via Microemulsion Method Using Orthogonal Experiment." *Crystals* **11**(11): 1387.
- Kalotra, S. and R. Mehta (2021).** "Synthesis of polyaniline/clay nanocomposites by in situ polymerization and its application for the removal of Acid Green 25 dye from wastewater." *Poly. Bulletin* **78**(5): 2439-2463.
- Kareem, A., N. Abd Alrazak, K. H. Aljebori, A. Aljebori, H. L. Algoory and A. F. Alkaim (2016).** "Removal of methylene blue dye from aqueous solutions by using activated carbon/ureaformaldehyde composite resin as an adsorbent." *Int. J. Chem. Sci.*, **14**(2): 635-648.
- Kooh, M. R. R., M. K. Dahri, L. Lim and L. L. Hoon (2017).** "Removal of acid blue 25 from aqueous solution by using common salts and seawater to induce the salting out effect." *Sci. Brun.*, **16** (2).
- Krishna, L. S., K. Soontarapa, N. K. Asmel, M. A. Kabir, Y. Ali, W. W. Zuhairi and Y. Sarala (2019).** "Adsorption of acid blue 25 from aqueous solution using zeolite and surfactant modified zeolite." *Desalin. Water Treat.*, **150**: 348-360.
- Kumar, K. Y., H. Muralidhara, Y. A. Nayaka, J. Balasubramanyam and H. Hanumanthappa (2013).** "Low-cost synthesis of metal oxide nanoparticles and their application in adsorption of commercial dye and heavy metal ion in aqueous solution." *Powder Tech.*, **246**: 125-136.
- Lakkaboyana, S. K., K. Soontarapa, R. K. Marella and K. Kannan (2021).** "Preparation of novel chitosan polymeric nanocomposite as an efficient material for the removal of Acid Blue 25 from aqueous environment." *Int. J. Biol. Macromol.* **168**: 760-768.
- Lin, G., H. Wang, X. Li, X. Lai, Y. Zou, X. Zhou, D. Liu, J. Wan and H. Xin (2018).** "Chestnut-like $\text{CoFe}_2\text{O}_4@ \text{SiO}_2@ \text{In}_2\text{O}_3$ nanocomposite microspheres with enhanced acetone sensing property." *Sensors Actuators B: Chem.* **255**: 3364-3373.
- Mahmoodi, N. M. (2014).** "Synthesis of core-shell magnetic adsorbent nanoparticle and selectivity analysis for binary system dye removal." *J. Ind. Eng. Chem.* **20**(4): 2050-2058.
- Mohanty, S. R. and S. K. Biswal (2022).** "An Overview of Removal of Heavy Metal Ions From Toxic Aqueous Solution Using Pani-Based Adsorbents." *Micro Nanosys.* **14**(2): 144-155.
- Nethaji, S., A. Sivasamy and A. Mandal (2013).** "Adsorption isotherms, kinetics and mechanism for the adsorption of cationic and anionic dyes onto carbonaceous particles prepared from Juglans regia shell biomass." *Inter. J Environ. Sci. Tech.* **10**(2): 231-242.
- Pan, Z., L. Qian, J. Shen, J. Huang, Y. Guo and Z. Zhang (2021).** "Construction and application of Z-scheme heterojunction $\text{In}_2\text{O}_3/\text{Bi}_4\text{O}_7$ with effective removal of antibiotic under visible light." *Chem. Eng. J.* **426**: 130385.
- Pantilimon, M. C., T. S. Kang and S.-J. Lee (2016).** "Synthesis of nano-sized indium oxide (In_2O_3) powder by a polymer solution route." *Ceram. Int.* **42**(3): 3762-3768.
- Salem, I. A., H. A. El-Ghamry and M. A. El-Ghobashy (2014).** "Catalytic decolorization of Acid blue 29 dye by H_2O_2 and a heterogeneous catalyst." *Beni-Suef Uni. J. Bas. App. Sci.*, **3**(3): 186-192.
- Salem, I. A., M. A. Salem and M. A. El-Ghobashy (2017).** "The dual role of

- ZnO nanoparticles for efficient capture of heavy metals and Acid blue 92 from water." *J. Mol. Liq.*, **248**: 527-538.
- Salem, M. A. (2010).** "The role of polyaniline salts in the removal of direct blue 78 from aqueous solution: A kinetic study." *React. Funct. Polym.*, **70**(10): 707-714.
- Salem, M. A., R. G. Elsharkawy, M. I. Ayad and M. Y. Elgendy (2019).** "Silver nanoparticles deposition on silica, magnetite, and alumina surfaces for effective removal of Allura red from aqueous solutions." *J. Sol-Gel Sci. Tech.*, **91**(3): 523-538.
- Salem, M. A., R. G. Elsharkawy and M. F. Hablas (2016).** "Adsorption of brilliant green dye by polyaniline/silver nanocomposite: Kinetic, equilibrium, and thermodynamic studies." *Eur. polym. J.*, **75**: 577-590.
- Samadi, A., M. Xie, J. Li, H. Shon, C. Zheng and S. Zhao (2021).** "Polyaniline-based adsorbents for aqueous pollutants removal: A review." *Chem. Eng. J.*, **418**: 129425.
- Senthilkumar, V., K. Senthil and P. Vickraman (2012).** "Microstructural, electrical and optical properties of indium tin oxide (ITO) nanoparticles synthesized by co-precipitation method." *Mater. Res. Bulletin*, **47**(4): 1051-1056.
- Sharma, D., H. S. Dutta and M. Dhayal (2022).** "Langmuir-Blodgett monolayer of electrochemically synthesized PANI-TiO₂ nanocomposites for MSG biosensor." *Appl. Surf. Sci.*, **10**: 100264.
- Skorb, E. V., E. A. Ustinovich, A. I. Kulak and D. V. Sviridov (2008).** "Photocatalytic activity of TiO₂: In₂O₃ nanocomposite films towards the degradation of arylmethane and azo dyes." *J. Photochem. Photobio. A: Chem.*, **193**(2-3): 97-102.
- Song, J., Y. Wei, M. Xu, J. Gao, L. Luo, H. Wu, X. Li, Y. Li and X. Wang (2022).** "Highly Sensitive Flexible Temperature Sensor Made Using PEDOT: PSS/PANI." *ACS App. Polym. Mater.*, **4**(2): 766-772.
- Sridhar B, C., J. Husain, M. Pradeep and M. Ambika Prasad (2016).** "Synthesis, characterization, electrical and sensor behavior of PANI/In₂O₃ nano composites." *Ferroelectr.*, **502**(1): 159-169.
- TaheriAshtiani, N. and B. Ayati (2022).** "Using chitosan-based heterogeneous catalyst for degradation of Acid Blue 25 in the effective electro-Fenton process with rotating cathodes." *J. Electro. Chem.*, **905**: 115983.
- Tanzifi, M. (2016).** "Removal of Congo Red Anionic Dye from Aqueous Solution Using Polyaniline/TiO₂ and Polypyrrole/TiO₂ Nanocomposites: Isotherm, Kinetic, and Thermodynamic Studies." *Inter. J. Eng.*, **29**(12): 1659-1669.
- Teng, X., M. Bryan, P. Chai and J. Law (2021).** "Preparation of polyaniline iron oxide composite (PANI/Fe₃O₄) for enhanced Congo red removal performance." *Mater. Today: Proc.*, **46**: 1875-1881.
- Tka, N., M. Jabli, T. A. Saleh and G. A. Salman (2018).** "Amines modified fibers obtained from natural Populus tremula and their rapid biosorption of Acid Blue 25." *J. Mol. Liq.*, **250**: 423-432.
- Xu, C., P. Qiu, H. Chen and F. Jiang (2017).** "Platinum modified indium oxide nanorods with enhanced photocatalytic activity on degradation of perfluorooctanoic acid (PFOA)." *J. Taiwan Inst. Chem. Eng.*, **80**: 761-768.
- Yakişik, H. and U. Özveren (2021).** "Synthesis of Polyaniline/Biochar composite material and modeling with nonlinear model for removal of copper (II) heavy metal ions." *J. Turk. Chem. Soc. A: Chem.*, **8**(1): 289-302.

- Yang, K., Z. Lao, F. Li, X. Liu, Y. Chen, Z. Zhang, K. Mai, Y. Zhang and X. Fan (2022). "A multi-functional model based on confined assembly of polyaniline on the surface of multiwalled carbon nanotubes as framework for high-performance lithium-sulfur battery." *Electrochimica Acta*, **415**: 140267.
- Yang, L., Y. Hong, E. Liu, X. Zhang, L. Wang, X. Lin and J. Shi (2021). "Significant enhancement of photocatalytic H₂ production simultaneous with dye degradation over Ni₂P modified In₂O₃ nanocomposites." *Sep. Purif. Tech.*, **263**: 118366.
- Zhang, W., L. Wang, Y. Su, Z. Liu and C. Du (2021). "Indium oxide/Halloysite composite as highly efficient adsorbent for tetracycline Removal: Key roles of hydroxyl groups and interfacial interaction." *Appl. Surf. Sci.*, **566**: 150708.
- Zhao, J., M. Zheng, X. Lai, H. Lu, N. Li, Z. Ling and J. Cao (2012). "Preparation of mesoporous In₂O₃ nanorods via a hydrothermal-annealing method and their gas sensing properties." *Mater. Lett.*, **75**: 126-129.
- Zhao, M., Z. Chen, X. Lv, K. Zhou, J. Zhang, X. Tian, X. Ren and X. Mei (2017). "Preparation of core-shell structured CaCO₃ microspheres as rapid and recyclable adsorbent for anionic dyes." *R. Soc. Health J.*, **4(9)**: 170697.

توليفة نانوية من أكسيد الإنديوم مع البولي أنيلين كمادة ماصة مبتكرة وفعالة لإزالة صبغة الحمض الأزرق ٢٥ من مياه الصرف

محمد السيد سالم^١ ، محمد أحمد الدمنهورى^١ ، أحمد محمد عمر^٢ ، مروه أبو اليزيد الغباشى^١

^١ قسم الكيمياء – كلية العلوم – جامعة طنطا - مصر

^٢ قسم بحوث المواد البوليمرية - معهد بحوث التكنولوجيا المتقدمة والمواد الجديدة - مدينة الأبحاث العلمية والتطبيقات التكنولوجية – مدينة برج العرب الجديدة - الإسكندرية - مصر

لقد إزداد خطر نفايات الأصباغ الإصطناعية الخطرة على البيئة المائية وصحة الإنسان بشكل سريع. لذلك تم تحضير توليفة نانوية من أكسيد الإنديوم المغلف بالبولي أنيلين (In₂O₃/PANI) لإزالة صبغة الحمض الأزرق ٢٥ الأنيونية الضارة (AB25) عن طريق الإمتزاز الحر المباشر. تم استخدام تقنيات التوصيف المختلفة لهذه التوليفة ومنها طيف امتصاص الأشعة تحت الحمراء ، حيود الأشعة السينية ، الميكروسكوب الإلكتروني الماسح والنافذ ، قياس المساحة السطحية للتوليفة ، طيف طاقة تشتت الأشعة السينية (FT-IR ، XRD ، SEM ، EDX ، BET ، TEM) للتحقق من أن التوليفة النانوية قد تم تحضيرها بنجاح. تتميز التوليفة المطورة بهيكل مسامي بمتوسط حجم الجسيم ٥٨.٤٣ نانومتر. أظهرت النتائج أن ٠.٠٠٧ جم فقط من التوليفة أزال ٩٥.٥٪ من الصبغة خلال ٩٠ دقيقة وأن نتائج الإمتزاز تتبع كيناتيكية نموذج الدرجة الثانية الزانفة. لقد وجد أن نتائج الإمتزاز تتطابق بدقة مع نماذج لانجمير وتوث للإمتزاز مع قدرة امتزاز قصوى بلغت ٢٥٣.٣٦ مجم/جم. أما من ناحية الديناميكا الحرارية وجد أن عملية الإمتزاز تلقائية وماصة للحرارة. من الجدير بالذكر أيضا أن التوليفة النانوية المحضرة أظهرت إنتقائية إمتزاز عالية تجاه صبغة AB25 الأنيونية مقارنة بصبغة الميثيلين الأزرق (MB) الكاتيونية. ومن المثير للإهتمام كذلك أن التوليفة احتفظت بخصائص امتزازية مرضية بعد خمس دورات متتالية من الاستخدام الفعال مع صبغة AB25 بنسبة إزالة تجاوزت ٨٣٪ مما يشير إلى أن هذه التوليفة خيار فعال وقابل للتطبيق للتخلص من الأصباغ الأنيونية الضارة من البيئة المائية.